Available online at www.sciencedirect.com
SCIENCE DIRECT
ELSEVIER
polymer
Polymer 46 (2005) 10290–10300
www.elsevier.com/locate/polymer

Crystallization, structure and properties of plasticized poly(L-lactide)

Z. Kulinski, E. Piorkowska*

Polymer Physics, Centre of Molecular and Macromolecular Studies, Polish Academy of Sciences, Sienkiewicza 112, 90 363 Lodz, Poland

Received 13 February 2005; received in revised form 26 July 2005; accepted 29 July 2005
Available online 25 August 2005

Abstract

Poly(L-lactide) (PLA) was plasticized with poly(ethylene glycol)s having M_w of 400 and 600 g/mol. In addition to poly(ethyne glycol)s with hydroxyl end groups, monomethyl ethers of poly(ethylene glycol) having M_w of 550 and 750 g/mol, with chains terminated with hydroxyl groups and methyl groups, were used. The effect of different end groups on the plasticization of both amorphous and semicrystalline PLA was studied. The crystallization, structure, thermal and tensile properties of PLA and PLA with 5 and 10 wt% of plasticizers were explored. No marked effect induced by different end groups of plasticizers was found. All the plasticizers used decreased T_g and increased the ability of PLA to cold crystallization. While an amorphous plasticized PLA could be deformed to about 550%, a semicrystalline PLA with the same total plasticizer content exhibited nonuniform plasticization of the amorphous phase and less ability to the plastic deformation. Nevertheless, a 20% elongation at break was achieved for a semicrystalline PLA with 10 wt% of the plasticizer. The plastic deformation of both neat and plasticized PLA was associated with crazing.

Keywords: Poly(L-lactide); Poly(ethylene glycol); Plasticization

1. Introduction

Poly(lactide) is a biodegradable polymer which can also be produced from annually renewable resources. This fact is responsible for a growing interest in poly(lactide) for many applications, as it is expected to reduce an impact on the environment caused by the production and utilization of petrochemical polymers. While expensive in the past, poly(lactide) becomes more competitive due to a recent development in polymerization technology [1].

Chiral center in the structure allows to vary the enantiomeric compositions of the poly(lactide). Both optically pure poly(L-lactide) and poly(D-lactide) are the crystallizable polymers. However, dimers of different chirality in the polymer chain lower its ability to crystallize. Beyond a certain concentration of the minor comonomer, crystallization does not occur [2]. In contrast, poly(L-lactide) and poly(D-lactide) cocrystallize into a stereocomplex which melts at temperature higher than that of the crystals of both enantiomers [3]. Different crystallinity levels can be reached depending on the molecular architecture and thermal history. Slowly crystallizing polylactides could be quenched below glass transition temperature and crystallized during subsequent heating [4].

Amorphous poly(L-lactide) (PLA) exhibits the glass transition temperature (T_g) in the range of 50–60 °C. Below that temperature PLA is rigid and brittle having the elastic modulus about 3 GPa and low ability to plastic deformation. Crystallinity, if developed, increases slightly the modulus of elasticity and further decreases the drawability [5]. To modify properties, PLA has been blended with other polymers including poly(3-methyl-1,4-dioxan-2-one) [6], starch [7,8], poly-ε-caprolactone [9], poly(vinyl acetate) [10], poly(methyl methacrylate) [11], poly(hydroxy butyrate) [12] and poly(ethylene oxide) [13]. Citrate esters [14, 15], triacetine [15] and poly(ethylene glycol) (PEG) [16–18] were found to be efficient plasticizers for PLA. Recent studies of PLA plasticized with PEG have demonstrated the increase in efficiency of plasticization with the decrease of PEG molecular weight; low molecular weight of the plasticizer enables increased miscibility with PLA and more efficient reduction of T_g. The transition from brittle do ductile behavior of the plasticized PLA occurs when T_g is shifted to 35 °C. The cold-crystallization temperature of PLA decreases in parallel with the shift in T_g [18]. These effects

* Corresponding author. Tel.: +48 42 6803223.
E-mail address: epiorkow@bilbo.cbmm.lodz.pl (E. Piorkowska).

0032-3861/$ - see front matter © 2005 Elsevier Ltd. All rights reserved.
doi:10.1016/j.polymer.2005.07.101

are enhanced not only by the lower molecular weight of PEG but also by its higher content. However, at a certain PEG content, dependent on its molecular weight, blends of PLA with PEG undergo a phase segregation. As it has been reported recently [19], blends of PLA of low stereoregularity with 30 wt% of PEG having molecular weight of 8000 g/mol are unstable due to slow crystallization of PEG that depletes the amorphous phase of the plasticizer. Blends of PLA of high stereoregularity with 30% of the same plasticizer undergo the phase separation with little or no crystallization [20].

Much less is known about the plasticizing effect of PEG on semicrystalline PLA. In studies devoted to the mechanical properties of plasticized PLA, its crystallization was rather a side effect that occurred at a relatively high plasticizer content, where PEG separation in the amorphous phase was also observed [17]. While the plasticizing effect of PEG on a semicrystalline PLA remains unclear, the crystallization of PLA/PEG blends was studied to some extent [16–18,21]. Recently, Lai et al. [22] have found that substitution of end hydroxyl groups by methyl groups in PEG with molecular weight of 2000 g/mol increased the miscibility of the plasticizer with PLA. The equilibrium melting temperature depression was more pronounced while acceleration of the spherulite growth rate was less affected by the plasticizer terminated with methyl groups than by that with hydroxyl groups. The influence of the plasticizer end groups on mechanical properties of the plasticized PLA was not reported in Ref. [22].

An upper temperature limit of applicability of an amorphous polymer is determined by its T_g, while that of a semicrystalline polymer by its melting temperature, usually much higher. Thus, effective plasticization of the amorphous phase of the semicrystalline polymer would greatly broaden the range of its potential applications. Also the migration of plasticizer molecules to a material surface [23], worsening the material properties, should be limited in the semicrystalline material.

The study is devoted to plasticization of the amorphous phase of semicrystalline PLA with poly(ethylene glycol) in order to obtain a material stable above T_g with an enhanced ability to the plastic deformation. In addition to PEG with hydroxyl end groups, monomethyl ether of poly(ethylene glycol), identical to PEG, except for that the chains are terminated with hydroxyl and also methyl groups, was used to determine the effect of different end groups on the mechanical properties of plasticized PLA. The thermal and mechanical properties as well as the structure of the amorphous and semicrystalline PLA with different plasticizer contents were studied and compared. The structure of the deformed plasticized PLA was also investigated to have an insight into the mechanism of the plastic deformation and failure. We have used PEGs with low molecular weight to achieve the effective plasticization at a relatively low content of the plasticizer, anticipating an increase of the plasticizer concentration in the amorphous phase during crystallization.

2. Experimental

The study utilized poly(L-lactide) manufactured by Cargill-Dow Inc., USA, with $M_w = 166{,}000$ g/mol, polydispersity $M_w/M_n = 2$, DLA content of 4.1%, and residual lactide content of 0.27%. Two PEGs with nominal M_w equal to 400 g/mol (P400) and to 600 g/mol (P600) were used as plasticizers. Two monomethyl ethers of poly(ethylene glycol) with nominal M_w of 550 g/mol (P550) and 750 g/mol (P750) were also applied to plasticize PLA.

The molecular weight of each plasticizer was characterized by Maldi time of flight method, in a linear mode, using a Voyager–Elite instrument (Perseptive Biosystems, USA) equipped with a pulsed N_2 laser. The matrix, 2,5-dihydroxybenzoic acid, and the cationizing agent, NaI, were dissolved in water.

Prior to blending, both polymers were vacuum dried at 100 °C for 4 h. Melt-blends containing 5 and 10 wt% of plasticizers and 0.3 wt% of Ultranox 626, added as a stabilizer, were prepared using a Brabender mixer operating at 190 °C for 20 min at 60 rpm, under the flow of dry gaseous nitrogen. These series of materials will be referred to as PLA-5 and PLA-10 through the paper, respectively. Neat PLA mixed with Ultranox 626 was also processed in the same way in order to obtain a reference material.

Differential scanning calorimetry (DSC) was carried out with a DSC TA Instrument 2920. Specimens weighing 10–12 mg were heated and cooled at the rate of 10 K/min. Subsequent heating and cooling runs were performed to verify the expected decrease of T_g and also to elaborate a protocol that allowed us to obtain samples either entirely amorphous or cold crystallized upon heating from the glassy state. It appeared that all the materials were amorphous after the processing. Cooling at the rate of 10 K/min was sufficiently fast to prevent PLA crystallization in all systems studied. PLA always crystallized upon the second heating. Stopping the heating beyond the crystallization peak, before the onset of melting, followed by cooling to room temperature allowed to obtain semicrystalline samples; no further crystallization was observed during the third heating. The only exception was the neat PLA which required isothermal annealing at the end of the second heating, prior to cooling, for completion of the crystallization.

According to the above findings, 0.3–0.4 mm thick entirely amorphous films of PLA and plasticized PLA were prepared by compression molding at 180 °C for 3 min in a hydraulic hot press followed by quenching between thick metal blocks kept at room temperature. Some of the amorphous films were cold-crystallized between two metal blocks equipped with heaters and Pt resistance thermometers connected to a temperature controller which enabled either heating or cooling of both blocks at the same programmed constant rate or holding steady temperature with an accuracy of 0.2 K. Good thermal contact between the sample and the blocks was achieved by slight pressing. The films were heated at the rate of 10 K/min from room temperature to a selected final temperature and quenched down to room temperature. The neat PLA films were kept at 137 °C for 75 min prior to quenching to allow the crystallization to complete.

The amorphous and semicrystalline films, as well as all four plasticizers used, were characterized by a DSC technique at the heating rate of 10 K/min. T_g of all the materials was measured as temperature corresponding to the midpoint of the heat capacity increment. In addition, measurements at the heating rate of 1 K/min, amplitude 0.106 K, and frequency 1/40 Hz were conducted in a TA Instruments Modulated DSC 2920 (MDSC).

To determine an average spherulite size in the semicrystalline neat and plasticized PLA, a small angle light scattering (SALS) method was employed. Thin films, 10–20 μm thick, were compression molded between microscope cover glasses. They were melt annealed for 3 min at 190 °C, quenched to room temperature and crystallized under the flow of gaseous nitrogen in a Linkam hot stage TMS92 mounted in a light microscope, employing the same protocol for temperature control as was used for the thick films. The SALS studies utilized a He–Ne laser as a light source with the wavelength of 0.6328 μm. Scattering patterns were recorded photographically. The light intensity distribution versus the scattering angle determined at the azimuthal angle of 45 °C was used for calculations of an average radius $\langle R \rangle$ [24].

The spherulite growth rate was measured during isothermal crystallization of the thin films at 130 °C. The films were melt annealed at 190 °C for 3 min and then cooled down to the crystallization temperature of 130 °C; it is already known [4] that such procedure leads to much less intense nucleation than that during cold crystallization. Several samples of each type were examined and an average value of the spherulite growth rate was calculated.

Dynamic mechanical properties were measured in the three point bending mode in a DMTA Mk III, Rheometric Scientific Ltd apparatus at the frequency of 1 Hz, on rectangular samples, 14 mm × 32 mm, cut from the amorphous and semicrystalline thick films.

Oar-shaped specimens, with 9.53 mm gauge length, and width of 3.18 mm, were cut from the thick films for tensile tests which were performed on an Instron tensile testing machine at room temperature, at the rate of 0.5 mm/min.

The gauge region of deformed samples was examined under a polarized light microscope with crossed polarizers. Specimens cut out from the gauge regions were studied in the DSC, at the heating rate of 10 K/min, and also in the MDSC.

The fracture surfaces of all materials were coated with gold and studied under a Jeol 5500 LV scanning electron microscope (SEM).

The crystal structure of semicrystalline films was probed by a wide angle X-ray diffraction (WAXS) in the reflection mode. A wide angle goniometer coupled to a sealed tube X-ray generator operating at 30 kV and 30 mA was used in this study. The X-ray beam consisted of Cu K_α radiation filtered by a Ni filter and electronically. The slit system that was used for collecting 2 theta scans, enabled the collection of the diffracted beam with a divergence angle of less than 0.05°.

The long period was determined by 2D small angle X-ray scattering (2D SAXS). A 1.1 m long Kiessig-type vacuum camera was equipped with a capillary collimator (X-Ray Optical Systems Inc.) and an imaging plate as a recording medium (Kodak). The camera was coupled to an X-ray generator (sealed-tube, fine point Cu K_α Ni filtered source operating at 50 kV and 35 mA, Philips). The capillary collimator enabled the resolution of scattering objects up to 40 nm. Exposed imaging plates were analyzed with PhosphorImager SI system (Molecular Dynamics).

3. Results

3.1. Characterization of plasticizers

M_w and M_w/M_n of the plasticizers measured by a Maldi TOF technique were: 417 g/mol and 1.06 for P400, 578 g/mol and 1.08 for P600, 551 g/mol and 1.12 for P550, 741 g/mol and 1.09 for P750, respectively. During heating in the DSC all four plasticizers exhibited melting below 50 °C, with the temperature of melting peak increasing with plasticizer molecular weight.

3.2. Characterization of neat and plasticized PLA

3.2.1. DSC and MDSC

Exemplary heating thermograms of the amorphous films are shown in Fig. 1. Above glass transition, the samples cold crystallized, and as temperature increased, melted. The amorphous PLA exhibited T_g around 57 °C, while the cold crystallization peak was centered at 120 °C. T_g decreased to 43–47 °C, and to 32–36 °C, for the amorphous PLA-5 and PLA-10, respectively. The cold crystallization peaks were narrowed and also shifted to lower temperature, from the range of 81–104 °C, depending on the plasticizer content, but independently of the plasticizer end groups. The long tails followed the crystallization peaks of PLA-5 and PLA-10 until melting. Melting of the neat PLA with the peak temperature at 151 °C, started before the completion of crystallization. On the thermograms of PLA-5 two pronounced melting peaks appeared; smaller at 141–146 °C, and larger at 152–155 °C. The increase of plasticizer content to 10 wt% decreased the smaller peak and shifted it to lower temperature, 133–140 °C, while the main peak at 150–154 °C was less affected.

On the DSC thermograms of crystallized films, shown in Fig. 2, glass transition is less pronounced than on the thermograms of amorphous films with the same compositions. This results not only from a decreased amount of the amorphous phase, but also from broadening of the transition

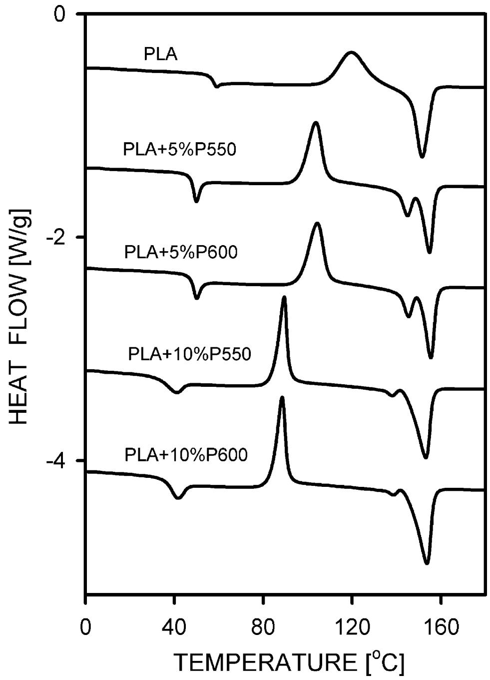

Fig. 1. DSC thermograms recorded during heating at the rate of 10 K/min for amorphous PLA and PLA plasticized with 5 and 10 wt% of P600 and P550. Thermograms are shifted along vertical axis.

clearly visible for the crystallized plasticized PLA. The T_g of the crystallized PLA increased by 1–2 K as compared with that of the amorphous PLA. The T_g of the crystallized PLA-5 was in the range of 35–37 °C. As the content of plasticizers increased to 10 wt%, the glass transition, beginning below room temperature, became very broad and nearly indistinguishable. However, the T_g of the crystallized PLA-10, taken as temperature of the midpoint of the heat capacity increment was lower only by 1–2 K than that of the crystallized PLA-5.

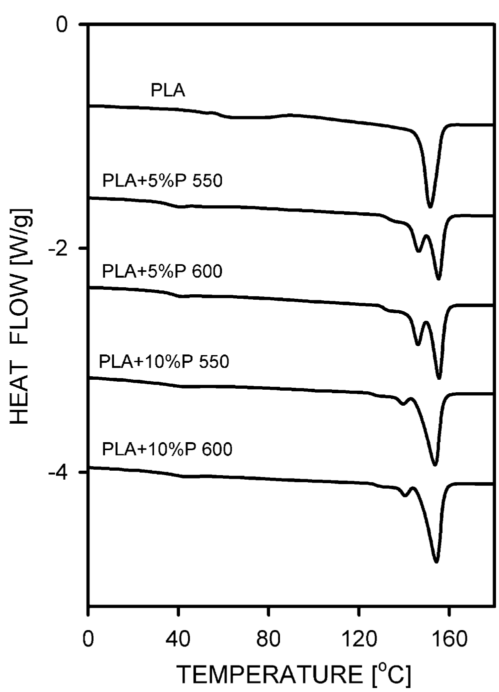

Fig. 2. DSC thermograms recorded during heating at the rate of 10 K/min for crystallized PLA and PLA plasticized with 5 and 10 wt% of P600 and P550. Thermograms are shifted along vertical axis.

The melting of crystallized neat and plasticized PLA started above 100 and 90 °C, respectively. The thermograms of crystallized PLA-5 and PLA-10 exhibited additional very small peaks, prior to the two higher melting peaks similar to those visible on the thermograms in Fig. 1; most probably they are connected with a minute fraction of thinner and/or less perfect crystals formed during quenching of the films to room temperature after cold crystallization.

Usually, crystallization enthalpy of the amorphous films corresponded to the melting enthalpy. The melting enthalpy in the range of 28–30 J/g increased slightly with broadening of temperature interval between the melting and crystallization that increased time available for completion of crystallization and further annealing. The melting enthalpy was about 42, 36 and 35 J/g for the semicrystalline PLA, PLA-5 and PLA-10, respectively. These values correspond to the crystallinity level of 40, 34 and 33%, respectively, if the enthalpy of fusion of 106 J/g is assumed [25].

Slower heating and temperature modulation employed in the MDSC experiment resulted in changes of the thermal transitions in the films studied as it is seen in Figs. 3 and 4. However, like in the ordinary DSC thermograms, the glass transition clearly visible in the reversing heat flow for the amorphous films, was less pronounced for the semicrystalline films; for crystallized PLA-10 it was hardly recognizable. The single melting peaks, visible on the thermograms of amorphous plasticized PLA in the total heat flow, centered around 156–157 °C, were preceded by the low and flat exotherms, while the additional melting peak appeared for neat PLA The reversing signal recorded for the

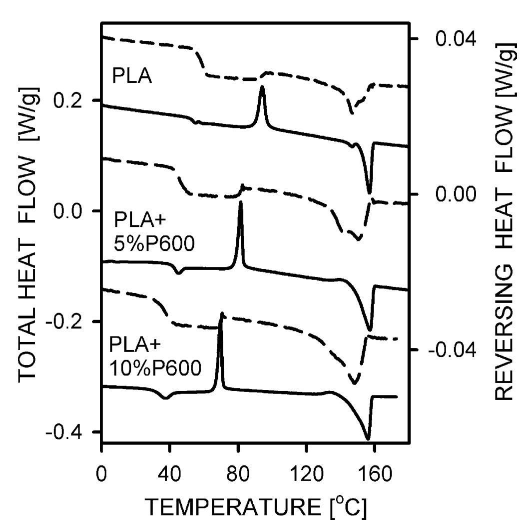

Fig. 3. MDSC thermograms recorded during heating at the rate of 1 K/min for amorphous: PLA, PLA with 5 wt% of P600 and PLA with 10 wt% of P600. Total heat flow, continuous line; reversing heat flow, dashed line. Thermograms are shifted along vertical axis.

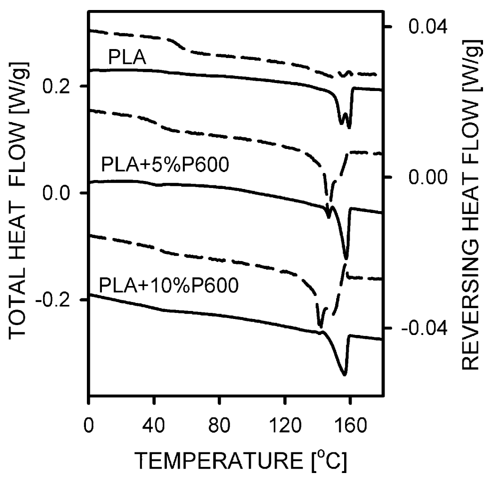

Fig. 4. MDSC thermograms recorded during heating at the rate of 1 K/min for crystallized: PLA, PLA with 5 wt% of P600 and PLA with 10 wt% of P600. Total heat flow, continuous line; reversing heat flow, dashed line. Thermograms are shifted along vertical axis.

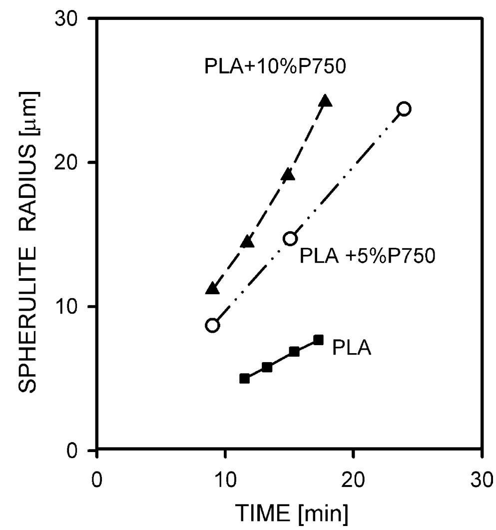

Fig. 5. Spherulite radius plotted against time during crystallization for neat PLA, PLA plasticized with 5 and 10 wt% of P750.

amorphous films exhibited pronounced peaks beyond the cold cystallization; the thermograms started to depart from the baseline at about 110–120 °C indicating the beginning of melting and recrystallization of PLA crystals.

The total heat flow recorded for the semicrystalline films exhibited the double melting peaks, although for the plasticized PLA the low temperature peaks were greatly decreased. The reversing signal indicated the recrystallization starting around 110–120 °C. The small peak temperatures of total signal recorded for crystallized PLA-5 and PLA-10 corresponded to the peak temperatures of reversing signal.

The DSC and MDSC measurements demonstrated also that the thermal properties of plasticized PLA are primarily governed by the plasticizer content and crystallinity while the influence of plasticizer end groups is not clearly recognizable.

3.2.2. Spherulite size and growth rate

An average spherulite radius, determined by SALS method was 1.8 μm in the PLA, and 1.5–2 μm in the crystallized plasticized PLA films. The spherulite growth rate at 130 °C was 0.46 μm/min for the neat PLA. For the PLA with 5 wt% of P600 and P750 the growth rate was 1.2 and 0.96 μm/min, respectively. As the plasticizer content increased to 10 wt%, the growth rate increased to 1.7 and 1.6 μm/min for the PLA with P600 and P750, respectively.

In the PLA and PLA-5 samples, spherulite radii were increasing proportionally with time, while in the measured PLA-10 samples the respective dependencies deviated from linearity, indicating the acceleration of growth with time, as it is shown in Fig. 5.

3.2.3. DMTA

Exemplary temperature dependencies of the loss modulus E'' and tan δ for the materials studied, are plotted in Figs. 6 and 7. The glass transition reflected in the E'' peaks and tan δ peaks is followed by cold crystallization of the amorphous materials. The plasticization decreased temperatures of both transitions to lower temperature, which was augmented by the higher plasticizer content. For the amorphous materials the E'' peak temperatures were very close, within an accuracy of 1–2 K, to the T_g values determined from the DSC experiments. The E'' peak temperature was equal to 58 and 60 °C for the amorphous and semicrystalline PLA, respectively, while the tan δ peak was at 65 °C for both. For the amorphous PLA-5 and PLA-10, the tan δ peak temperature was decreased to 55–56 and 45–47 °C, respectively.

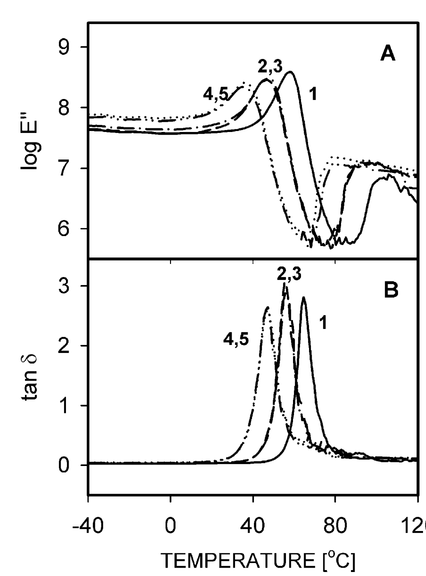

Fig. 6. Temperature dependence of dynamic mechanical properties of amorphous PLA and PLA plasticized with P600 and P750: log E'' (A) and tan δ (B). 1, PLA; 2, PLA with 5 wt% of P600; 3, PLA with 5 wt% of P750; 4, PLA with 10 wt% of P600; 5, PLA with 10 wt% of P750.

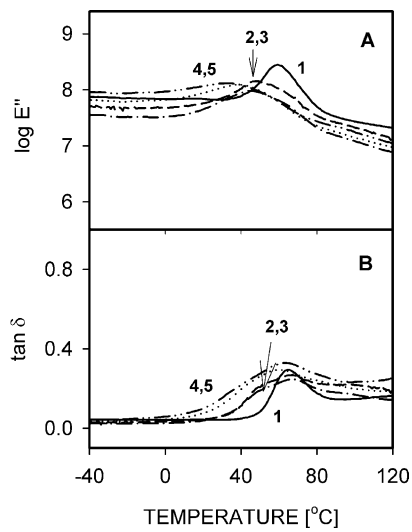

Fig. 7. Temperature dependence of dynamic mechanical properties of crystallized PLA and PLA plasticized with P600 and P750: log E'' (A) and tan δ (B). 1, PLA; 2, PLA with 5 wt% of P600; 3, PLA with 5 wt% of P750; 4, PLA with 10 wt% of P600; 5, PLA with 10 wt% of P750.

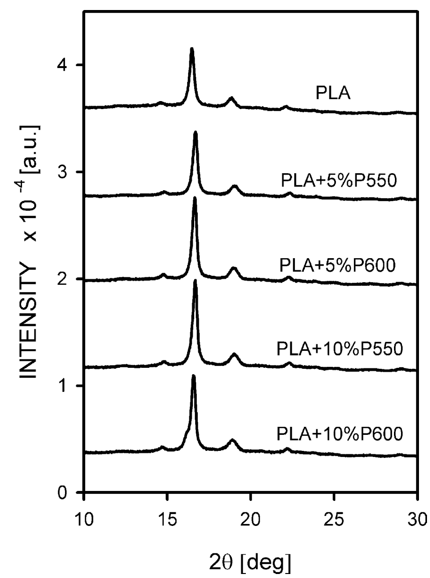

Fig. 8. X-ray diffractograms of crystallized neat PLA, PLA with 5 wt% of P550, PLA with 5 wt% of P600, PLA with 10 wt% of 550 and PLA with 10 wt% of 600. Curves are shifted along vertical axis.

While for the crystallized PLA-5 the E'' peak temperatures were lower by 3 K than those for the amorphous PLA-5, the differences disappeared for the PLA-10 films.The E'' peak temperatures of the crystallized plasticized PLA films exceeded also the T_g values determined by the DSC method, however, more for the PLA-5 films. The tan δ peak temperatures were higher than for the amorphous plasticized PLA. For the semicrystalline films, the E'' peaks and, especially, the tan δ peaks were broader and much lower than for the amorphous materials indicating that the plasticization of semicrystalline PLA resulted in the marked broadening of the glass transition augmented by the higher plasticizer content.

There was no significant difference between the results obtained for plasticizers with different end groups; the glass transition was affected primarily by the plasticizer content and crystallinity.

3.2.4. X-ray studies

Exemplary 2 theta scans for the crystallized films, depicted in Fig. 8, reveal peaks typical of α-form described as pseudo-orthorhombic [26], pseudo-hexagonal [27] or orthorhombic [28]. The long period determined by the SAXS method is about 21 nm for PLA, 17.5–19 and 15.5–16.5 nm for PLA-5 and PLA-10, respectively.

The decrease of long period together with the decrease of crystallinity level measured for those materials by the DSC technique indicated the slight decrease of an average lamellae thickness in the plasticized PLA.

3.2.5. Tensile properties

The results of tensile tests are collected in Figs. 9 and 10. While the crystallized PLA fractured before a yield, the amorphous PLA yielded at the deformation about 5% and the stress of 47 MPa and exhibited some ability to the plastic flow; the average elongation and stress at break were around 18% and 41 MPa, respectively. Five weight percent of plasticizer caused the decrease of the yield stress of amorphous samples to 35–39 MPa. The stress at break of the amorphous PLA-5 materials was in the range of 25–27 MPa, while the average elongation at break was

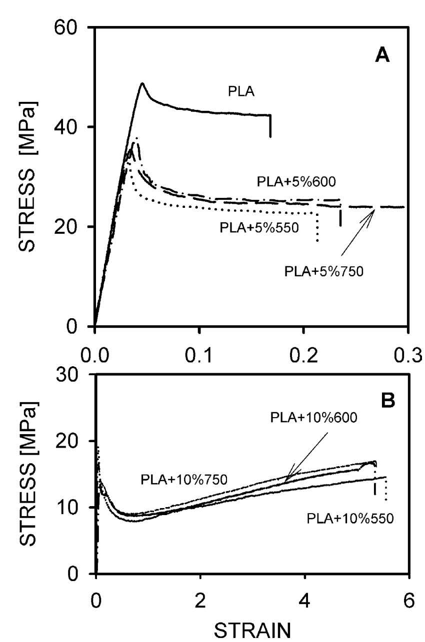

Fig. 9. Stress–strain dependencies for amorphous neat PLA, PLA with 5 wt% of P550, PLA with 5 wt% of P600, PLA with 5 wt% of P750 (A), PLA 10 wt% with of P550, PLA with 10 wt% of P600 and PLA with 10 wt% of P750 (B).

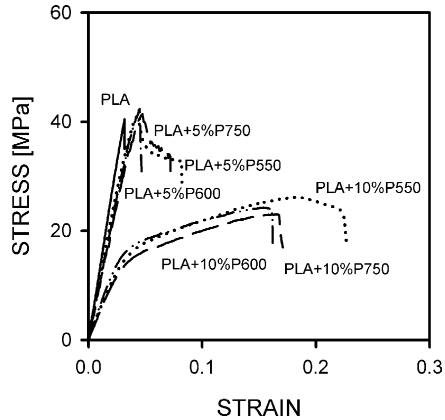

Fig. 10. Stress–strain dependencies for cold crystallized neat PLA, PLA with 5 wt% of P550, PLA with 5 wt% of P600, PLA with 5 wt% of P750, PLA with 10 wt% of P550 and PLA with 5 wt% of P600 and PLA with10 wt% of P750.

between 10 and 22%, however, the maximum elongation usually exceeded 20%. The increase of plasticizer content to 10 wt% further decreased the yield stress to about 18–20 MPa, and dramatically increased the elongation at break which exceeded 550% for the amorphous specimens of PLA with P550, P600 and P750, while 300% for PLA with P400. For the amorphous PLA-10 after the yield, the stress sharply declined but then increased gradually to 16–18 MPa, as it is visible in Fig. 10. The crystallized PLA-5 specimens yielded at about 39 MPa and fractured early, at the average elongation between 5 and 11% and at the stress around 33 MPa. The increase of the plasticizer content to 10 wt% further modified the behavior of the semicrystalline specimens. The yield point, below 20 MPa, less pronounced than for the other materials, was followed by the gradual increase of the flow stress. The average elongation at break was within a range of 16–22%, while the stress at break was around 22–23 MPa, with the exception of PLA with P400, which fractured early, at the elongation of 4.5%.

3.2.6. Polarized light microscopy of deformed samples

Fig. 11 shows typical light micrographs of the gauge regions of the specimens deformed to fracture. In the micrographs of amorphous PLA and PLA with 5 wt% of P550 a relatively uniform distribution of whitened craze zones is visible. The micrograph of semicrystalline PLA with 5 wt% of P550 shows the black fissures propagating perpendicularly to the drawing direction which are most probably also crazes. The amorphous PLA with 10 wt% of P600 (Fig. 11(D)) after deformation exhibited stress-whitening and brightening under a light microscope. In this specimen short black lines perpendicular to the drawing direction, with brightened edges, resembling short crazes, are discernible. In the crystallized PLA and PLA-10 no evident features related to the deformation were found by a light microscopy. Fig. 12 shows micrographs of the gauge region of amorphous PLA with 10 wt% of P750 strained to

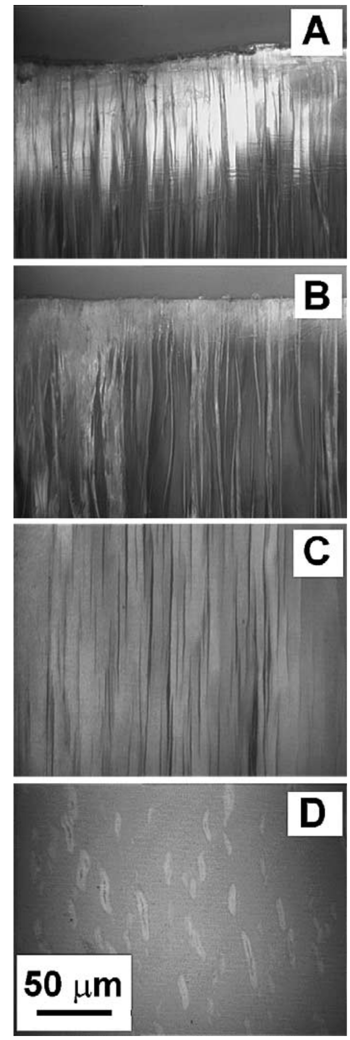

Fig. 11. Polarized light micrographs of the gauge regions of amorphous PLA (A), amorphous PLA with 5 wt% of P550 (B), cold crystallized PLA with 5 wt% of P550 (C) and initially amorphous PLA with 10 wt% of P600. (D) Crossed polarizers. Drawing direction, horizontal.

20% and to 100%. In the samples strained to 20% an intense cavitation and also local increase of transmitted light intensity through crossed polarizers are visible indicating the orientation and possible crystallization of PLA. At the strain of 100% the entire sample is brightened; besides, numerous cavities are discernible, some of them connected.

3.2.7. SEM of fracture surfaces

Typical micrographs of the fracture surfaces of amorphous and semicrystalline specimens are shown in Figs. 13 and 14, respectively. The micrographs of amorphous PLA and PLA with 5 wt% of P600 reveal rather brittle fracture surfaces with little plastic deformation; few long threads of a deformed material are discernible on the fracture surfaces of these materials. On the entire fracture surfaces of the initially amorphous specimen of PLA with 10 wt% of P600, shown in Fig. 13(C), a large amount of plastically deformed material is visible. The surface of

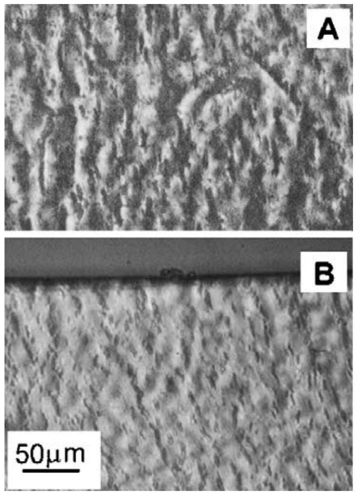

Fig. 12. Polarized light micrographs of the gauge regions of amorphous PLA with 10 wt% of P750 deformed to 20% (A) and to100% (B). Crossed polarizers. Drawing direction, horizontal.

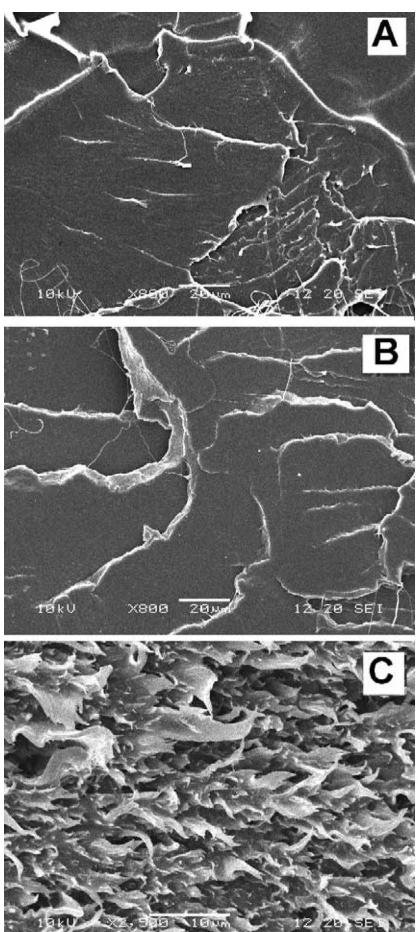

Fig. 13. SEM micrographs of fracture surfaces of amorphous neat PLA (A), PLA with 5 wt% of P600 (B) and PLA with 10 wt% of P600 (C).

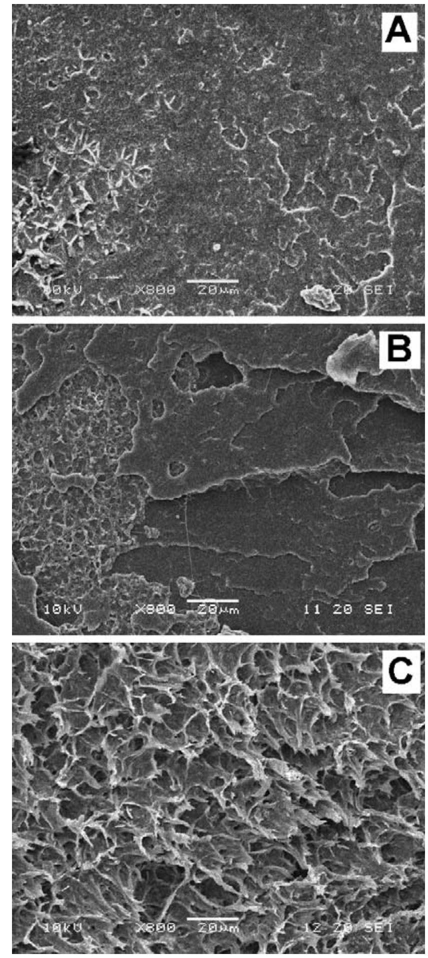

Fig. 14. SEM micrographs of fracture surfaces of semicrystalline neat PLA (A), PLA with 5 wt% of P750 (B) and PLA with 10 wt% of P600 (C).

crystallized PLA, shown in Fig. 14(A), exhibits features of brittle fracture although on a micro-scale some development of the fracture surface is visible. Others interpret such patterns as a result of craze fracture [29]. On the fracture surfaces of semicrystalline PLA with 5 wt% of P750, beside areas indicating brittle fracture also the areas with dimple patterns of hollows surrounded by plastically deformed walls are distinguishable (Fig. 14(B)). Fig. 14(C) demonstrates the dimple pattern prevailing on the fracture surfaces of semicrystalline PLA-10. The walls surrounding cells are much more deformed than those visible on the fracture surfaces of PLA-5. The cell diameter is of the order of an average spherulite size as measured by the SALS method. Dimple patterns, like those in Fig. 14(C), were already found by others in semicrystalline polymers and attributed to a fracture of strained craze fibrils [29,30].

3.2.8. DSC and MDSC of deformed samples

Heating scans, at the rate of 10 K/min, of the samples cut after fracture from gauge regions of the initially amorphous PLA-10 specimens differ markedly from the scans of the respective films prior to the deformation, as it is shown in

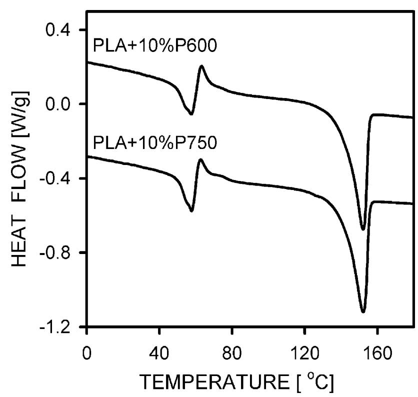

Fig. 15. DSC thermograms recorded during heating at the rate of 10 K/min of initially amorphous PLA with 10 wt% of P600 and PLA with 10 wt% of P750 after deformation. Plots are shifted along vertical axis.

Fig. 15. On these thermograms the pronounced glass transition was associated with a very intense enthalpy relaxation, and followed by a small exothermic peak, of few J/g, probably due to crystallization. The material was strained to more than 550% prior to heating in the DSC, thus stress relaxation phenomena can also influence the thermogram above T_g. The melting peak centered about 150–152 °C was associated with the enthalpy of melting of about 39 J/g. Thus, the deformation of amorphous PLA-10 leads to the strain induced crystallization. The melting temperature of crystals formed during drawing was slightly below the melting peak temperatures of the same materials cold crystallized under quiescent mechanical conditions. The melting peaks of MDSC total heat flow (Fig. 16) were centered about 155–156 °C due to slow heating and recrystallization, the latter visible in the reversing signal. The reversing signal reflected clearly the glass transition, unlike in the materials with the same compositions crystallized in quiescent conditions. The T_g of 46–49 °C, determined from the reversing signal exceeded by several degrees the T_g measured prior to the deformation by the same method. X-ray diffraction of the gauge regions of initially amorphous PLA-10 after fracture confirmed the presence of oriented α-orthorhombic form.

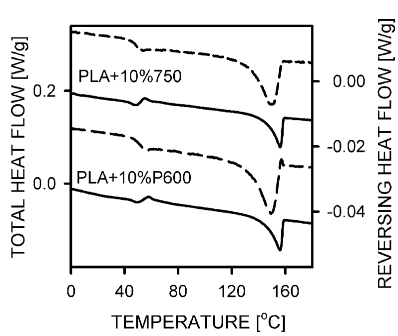

Fig. 16. MDSC thermograms recorded during heating at the rate of 1 K/min of initially amorphous plasticized PLA with 10 wt% of P750 and PLA with 10 wt% of P600 after deformation. Total heat flow, continuous line; reversing heat flow, dashed line. Thermograms are shifted along vertical axis.

4. Discussion and conclusions

The plasticization of the PLA with poly(ethylene glycol) and monomethyl ether of poly(ethylene glycol) effectively lowers T_g. The DSC and DMTA data for the amorphous PLA show clearly a decrease of T_g due to enhanced segmental mobility of PLA chains caused by the presence of plasticizers, increasing with the plasticizer content. No trace of separate melting or crystallization of PEG was found confirming that the phase separation of PEG did not occur. No significant differences were found due to the different chain end groups of the plasticizers used.

The plasticizers increased the ability of PLA to crystallize as it was already reported [18,22]; the temperature of cold crystallization was decreased and the crystallization peak was narrowed, which was again enhanced by the higher plasticizer content and also by the lower heating rate. The overall crystallization kinetics always depends on the spherulite nucleation and, to a larger extent, on the spherulite growth rate. The average spherulite size in the cold crystallized samples as determined by the SALS method was not affected significantly by the plasticization. Lai et al. [22] found only a minor decrease in the number of spherulite nuclei during isothermal crystallization of PLA caused by addition of 10 wt% of PEG terminated with two –OH groups and also in the case when one –OH is replaced by $–CH_3$ group. On the contrary, the spherulite growth rate increased due to plasticization. In Ref. [22] it was explained as the effect of an increased segmental mobility and decreased surface energy of lamellae overcoming the depression of equilibrium melting point and the dilution of PLA. The crystallographic α-form of PLA crystals was preserved in the plasticized materials, but the long period and lamella thickness decreased somewhat in the presence of plasticizers. This can be understood as the effect related to a strong reduction of surface energy, especially, the fold surface energy (proved in Ref.[22]) and also to a decreased undercooling.

The melting behaviour of the materials studied depended on their composition but, also on a heating rate during crystallization and during melting as well. Others already explained the additional melting peaks appearing on DSC thermograms of plasticized PLA as related to the reorganization of crystal structure [13]. The MDSC heating scans carried out in the present study confirmed the lamellae reorganization in the plasticized PLA reflected in reversing signal. As the plasticizers utilized in the study do not cocrystallize with PLA, their average concentration in the amorphous phase increased during PLA crystallization from 5 to 7.5 wt% in PLA-5 and from 10 to 15 wt% in PLA-10, as was calculated based on the crystallinity level achieved in these materials. The DSC results demonstrated that after the crystallization the T_g value was lowered and the glass transition became broader, the latter especially in PLA-10. DMTA curves showed very clearly the broadening of glass transition after crystallization, visible already for PLA-5, and enhanced for PLA-10. Thus, while the glass transition in the amorphous plasticized PLA was shifted to lower temperature, in the crystallized plasticized PLA it was shifted less but markedly broadened which might be attributed to a varying plasticizer content in the amorphous phase.

The acceleration of spherulite growth rate found in PLA-10 confirmed the tendency of the plasticizers to accumulate in front of growing spherulite that was a result of segregation during the crystallization. Although Lai et al. [22] did not report such phenomenon, it might be enhanced by the plasticizer lower molecular weight enabling its easier migration from intraspherulitic amorphous layers to the surrounding melt [31].

The tensile properties demonstrated that the plasticizers enhancing the segmental mobility of PLA chains increased the ability of amorphous PLA to the plastic deformation, decreasing the yield stress and increasing the elongation at break as it was reported in Ref. [16–18]. Light microscopy demonstrated clearly that in the PLA and PLA-5, where the T_g is still above room temperature, the plastic deformation was due to crazing, similarly as in other glassy polymers. However, one might expect that the ability of PLA to crystallize affected the mechanism of craze width growth and craze fibril breakdown. The mechanism of plastic deformation in the amorphous PLA-10 is obviously more complicated. The short crazes, discernible under a light microscope in the PLA10 specimens strained to fracture differ from those found in the PLA and PLA-5. It is already known that glassy polymer-diluent mixtures deformed in a temperature range close to T_g, are inclined to exhibit a cavitational mode of plasticity because the diluent enhances the chain slippage required for the formation of craze fibrils [32]. While both the deformation process and the structure of oriented PLA-10 require further studies, it was established that the plastic deformation is associated with cavitation and also with strain-induced crystallization of PLA. No evidence of the formation of β-crystallographic form in those samples was found, similarly as it was reported for the neat PLA drawn slightly above T_g, which crystallized in α-form [33]. The glass transition in the oriented, strain crystallized PLA-10 studied by the calorimetric methods was more pronounced and less diffuse than in the PLA-10 crystallized under quiescent conditions in the spherulitic form.

The cold crystallization diminished the drawability of both neat and plasticized PLA. In the crystallized PLA-5, the yield stress increased by a few MPa and the elongation at break decreased about two times with respect to the amorphous PLA-5. The onset of plastic deformation in the crystallized PLA-10 occurred at the stress somewhat lower than that measured for the amorphous PLA-10. However, the stress at break was nearly two times higher and the elongation at break was one order of magnitude less than that achieved for amorphous PLA-10.

The fracture occurred in a brittle manner in the crystallized neat PLA; features related to the fracture of crazes were found by the SEM technique. Dimple patterns appeared on the fracture surfaces of crystallized PLA-5 and became a dominant feature of the fracture surfaces of crystallized PLA-10 in contrast to rather uniformly distributed fibrils of deformed materials visible in the case of initially amorphous PLA-10 specimens. The deformation of cell walls, as observed by SEM in the crystallized plasticized PLA intensified with the increase of the plasticizer content. Dimple patterns found on fracture surfaces of other semicrystalline polymers are attributed to straining craze fibrils to fracture [29,30]. Thus, the light microscopy and SEM results allow us to conclude that the mechanism of the plastic deformation in the semicrystalline plasticized PLA is also associated with crazing, although crazes in semicrystalline polymers, designated also in the literature as micronecks and fibrillar deformation zones, differ significantly from crazes in glassy amorphous polymers.

It was established in the past that a low crystallinity level and fine spherulitic structure, like those in the PLA studied, were advantageous for development of crazes in the semicrystalline polymers [31]. Unlike in the amorphous polymers, crazing in the semicrystalline polymers is not restricted to temperatures below T_g but occurs also above the glass transition of the amorphous phase [34]. Below T_g, long crazes propagate perpendicularly to load direction ignoring the internal polymer structure, while at temperature close to T_g the crazes are confined to several spherulites [29,30]. Long crazes revealed in PLA-5 materials by the light microscopy conform to this picture as T_g of those materials remains still above room temperature. With the increase of plasticizer content to 10 wt%, which shifts the onset of glass transition below room temperature, the second scenario becomes more probable. The plasticization enhancing the segmental mobility of chains and enabling easier chain slippage promoted the craze formation within the amorphous phase. The hollows in dimple patterns resulted from earlier fracture of craze fibrils in those areas. In a spherulitic sample the local strains and stresses within the sample differ due to different orientation of lamellae with respect to the principal stress direction that might contribute to localized fracture initiation. As it was found based on the DSC, MDSC and DMTA measurements, the plasticization of semicrystalline PLA was less uniform than in the case of amorphous PLA. The spherulite growth rate measurements indicated that segregation of the plasticizers led to a gradient of plasticizer concentration along the spherulite radius. The nonuniform plasticization might also contribute to early fracture of the crystallized plasticized PLA, especially that sizes of cells visible on the fracture surfaces were of the same order of magnitude as was the average spherulite size.

Nevertheless, the plasticized semicrystalline samples gained the ability to plastic deformation, leading to about 20% elongation at break in the case of 10 wt% plasticizer content. The advantage of semicrystalline materials is that the temperature range of their possible application is limited by the melting temperature, which remains high, at 150–160 °C, while for entirely amorphous PLA based materials the limiting temperature is T_g, which is much lower, below 60 °C.

No clear influence of the plasticizer end group on thermal transition temperatures and other properties of the plasticized PLA was found; instead the properties were rather governed by the plasticizer content. We have, however, to point out that the plasticizers used by us differed in one chain-end group only and the total plasticizer content did not exceed 10 wt%, while in Ref. [22] where the influence of PEG end group was studied, the PEGs with two methyl groups were also used and PEG concentration reached 70 wt%.

Acknowledgements

This work was partially supported by the Ministry of Science and Information Society Technologies (Poland) through the Centre of Molecular and Macromolecular Studies, PAS, under Grant PBZ KBN 070/T09/2001, 2003–2006. The authors gratefully acknowledge the Cargill-Dow Polymers, LLC, for supplying PLA.

References

[1] Jacobsen S, Degee Ph, Fritz HG, Dubois PhL, Jerome R. Polym Eng Sci 1999;39:1311.
[2] Brochu S, Prud'homme RE, Barakat I, Jerome P. Macromolecules 1995;28:5230.
[3] Brizzolara D, Cantow HJ, Diederichs K, Keller E, Domb AJ. Macromolecules 1996;29:191.
[4] Pluta M, Galeski A. J Appl Polym Sci 2002;86:1386.
[5] Perego G, Cella GD, Bastioli C. J Appl Polym Sci 1996;59:37.
[6] Bechtold K, Hillmyer MA, Tolman WB. Macromolecules 2001;34:8641.
[7] Park JW, Im SS. Polym Eng Sci 2000;40:2539.
[8] Martin O, Averous L. Polymer 2001;42:6209.
[9] Cohen D, Younes HJ. Biomed Mater Res 1988;22:993.
[10] Gajria A, Dave V, Gross RA, McCarthy SP. Polymer 1996;37:437.
[11] Eguiburu JL, Iruin JJ, Fernandez-Berridi MJ, Roman JS. Polymer 1998;39:6891.
[12] Focarete ML, Ceccourulli G, Scandola M, Kowalczuk M. Macromolecules 1998;31:8485.
[13] Nijenhuis AJ, Colstee E, Grijpma DW, Pennings AJ. Polymer 1996;37:5849.
[14] Labrecque LV, Kumar RA, Dave V, Gross RA, McCarthy SP. J Appl Polym Sci 1997;66:1507.
[15] Ljungberg N, Wesselen B. J Appl Polym Sci 2002;86:1227.
[16] Jacobsen S, Fritz HG. Polym Eng Sci 1999;39:1303.
[17] Sheth M, Kumar RA, Dave V, Gross AR, McCarthy SP. J Appl Polym Sci 1997;66:1495.
[18] Baiardo M, Frisoni G, Scandola M, Rimelen M, Lips D, Ruffieux K, et al. J Appl Polym Sci 2003;90:1731.
[19] Hu Y, Rogunova M, Topolkaraev V, Hiltner A, Baer E. Polymer 2003;44:5701.
[20] Hu Y, Hu YS, Topolkaraev V, Hiltner A, Baer E. Polymer 2003;44:5711.
[21] Hu Y, Hu YS, Topolkaraev V, Hiltner A, Baer E. Polymer 2003;44:5681.
[22] Lai WCh, Liau WB, Lin TT. Polymer 2004;45:3073.
[23] Pluta M, Paul MA, Alexandre M, Dubois PhL. J Polym Sci Part B: Polym Phys; submitted for publication.
[24] Stein RS, Rhodes MB. J Appl Phys 1960;31:1873.
[25] Sarasua JR, Prud'homme RE, Wisniewski M, Le Borgne A, Spassky N. Macromolecules 1998;31:3895.
[26] DeSantis P, Kovacs AJ. Biopolymers 1968;6:299.
[27] Hoogsteen W, Postema AR, Pennings AJ, Brinke GT, Zugenmaier P. Macromolecules 1990;23:634.
[28] Miyata T, Masuko T. Polymer 1997;38:4003.
[29] Friedrich K. Adv Polym Sci 1983;52/53:225.
[30] Narisawa I, Ishikawa M. Adv Polym Sci 1990;91/92:353.
[31] Keith HD, Padden Jr FJ. J Appl Phys 1964;35:1270.
[32] Dettenmaier M, Leberger D. Adv Polym Sci 1990;91/92:119.
[33] Sawai D, Takayashi K, Imamura T, Nakamura K, Kanamoto T, Hyon SH. J Polym Sci, Part B: Polym Phys 2002;40:95.
[34] Kausch HH, Gensler R, Grein C, Plummer CJG, Scaramuzzino P. J Macromol Sci, Phys 1999;B38:803.